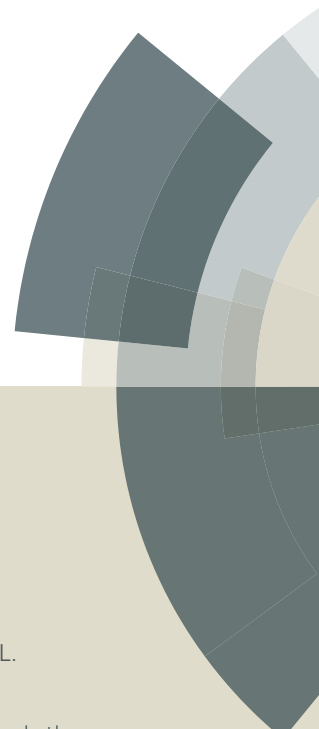


# Photochemical & Photobiological Sciences

Accepted Manuscript



This article can be cited before page numbers have been issued, to do this please use: M. A. Orellana, L. Osiglio, P. Arnal and L. R. Pizzio, *Photochem. Photobiol. Sci.*, 2016, DOI: 10.1039/C6PP00175K.



This is an *Accepted Manuscript*, which has been through the Royal Society of Chemistry peer review process and has been accepted for publication.

*Accepted Manuscripts* are published online shortly after acceptance, before technical editing, formatting and proof reading. Using this free service, authors can make their results available to the community, in citable form, before we publish the edited article. We will replace this *Accepted Manuscript* with the edited and formatted *Advance Article* as soon as it is available.

You can find more information about *Accepted Manuscripts* in the [Information for Authors](#).

Please note that technical editing may introduce minor changes to the text and/or graphics, which may alter content. The journal's standard [Terms & Conditions](#) and the [Ethical guidelines](#) still apply. In no event shall the Royal Society of Chemistry be held responsible for any errors or omissions in this *Accepted Manuscript* or any consequences arising from the use of any information it contains.



## Journal Name

## ARTICLE

## Titania hollow spheres modified with tungstophosphoric acid with enhanced visible light absorption for the photodegradation of 4-chlorophenol

M.Á. Orellana<sup>a</sup>, L. Osiglio<sup>a</sup>, P.M. Arnal<sup>b</sup> and L.R. Pizzio<sup>a</sup>

Received 00th January 20xx,  
Accepted 00th January 20xx

DOI: 10.1039/x0xx00000x

www.rsc.org/

Titania hollow spheres were synthesized using silica nanospheres as template. The core was removed using NaOH solution. They were subsequently impregnated with tungstophosphoric acid (TPA) solutions and annealed at two different temperatures (100 and 500 °C). These materials were characterized by several physicochemical techniques (XRD, BET, SEM, DRS, FT-IR, FT-Raman and <sup>31</sup>P MAS-NMR). The <sup>31</sup>P MAS-NMR and FT-IR characterization showed that the main species present in the samples is the [PW<sub>12</sub>O<sub>40</sub>]<sup>3-</sup> anion, which was partially transformed into [P<sub>2</sub>W<sub>21</sub>O<sub>71</sub>]<sup>6-</sup> anion during the synthesis and drying step. <sup>31</sup>P MAS-NMR, and FT-Raman characterization revealed evidence of a strong interaction between the Keggin anion of TPA and TiO<sub>2</sub> surfaces, possibly due to the formation of surface heteropolyacid-TiO<sub>2</sub> complexes. The DRS results showed that the absorption threshold onset continuously shifted to the visible region with increased TPA concentration and calcination at 500 °C. The enhanced visible light absorption could be related to the formation of a surface complex TPA Keggin anion-TiO<sub>2</sub>. The catalytic activity of the materials in the photodegradation of 4-chlorophenol under UV and visible light irradiations increased when the TPA content and the calcination temperature of the samples were raised.

### 1. Introduction

The potential of heterogeneous photocatalysis over TiO<sub>2</sub> to destroy a wide range of waterborne pollutants and microorganisms has aroused enormous interest.<sup>1,2</sup> The preparation of titania-based photocatalysts with high catalytic performance has also attracted much attention. TiO<sub>2</sub> has been the most widely used because it is easily available, inexpensive, nontoxic, and shows relatively high chemical stability.<sup>3</sup>

It is claimed that titania performance in the photodegradation of contaminants contained in wastes depends on its crystal structure, crystallinity, surface area, surface hydroxyl density, band gap energy, and morphology,<sup>4</sup> among other factors. The low surface area and the fast recombination of the photoinduced electrons and holes are the main effects that can lead to a low photocatalytic activity. Additionally, titania absorbs only UV light, which is not abundant on the earth's surface, representing an enormous limitation in solar-driven photocatalytic processes.

In the last years, the synthesis of titania hollow microspheres (@TiO<sub>2</sub>) has attracted much attention due to their large surface

area, low density, and highly efficient light-harvesting properties.<sup>5-9</sup> They were successfully synthesized using pentahydrated copper sulfate<sup>6</sup>, latex<sup>7</sup> or silica<sup>9,10</sup> spheres as templates. The synthesis using a template free solvothermal method has been also informed.<sup>8</sup>

Additionally, shell and core-shell particles (@TiO<sub>2</sub> and SiO<sub>2</sub>@TiO<sub>2</sub>, respectively) may be less harmful to biological systems than TiO<sub>2</sub> nanoparticles.<sup>10</sup>

Tungstophosphoric and tungstosilicic acid (TPA and TSA, respectively) were employed as effective homogeneous photocatalysts in the degradation of organic pollutants in water. They have been also used to modify TiO<sub>2</sub> in order to reduce the charge recombination and enhance visible light absorption.<sup>3</sup>

The photocatalytic degradation of 4-chlorophenol (4-CP) has been investigated by many research groups and has become a standard reaction for evaluating various experimental parameters in photocatalysis.<sup>11-13</sup>

We present here, for first time, the preparation and characterization of titania hollow microspheres modified with TPA. The influence of some preparation conditions on the catalytic activity in 4-CP photodegradation was studied.

<sup>a</sup> Centro de Investigación y Desarrollo en Ciencias Aplicadas "Dr. Jorge J. Ronco" (CINDECA), Facultad de Ciencias Exactas, UNLP-CCT La Plata, CONICET, 47 N° 257, 1900-La Plata, Argentina. E-mail: lrpizzio@química.unlp.edu.ar

<sup>b</sup> CETMIC, Centro de Tecnología de Recursos Minerales y Cerámica, CIC-CONICET Gonnet, La Plata, Argentina.

## 2. Experimental section

### 2.1. Catalysts synthesis

Nano spherical particles with an amorphous, solid core of SiO<sub>2</sub> and a porous, polycrystalline shell of TiO<sub>2</sub> were formed in a three-step procedure.<sup>10</sup> The first step yielded silica spheres, the second step, silica spheres covered with a layer of amorphous titanium oxide (SiO<sub>2</sub>@TiO<sub>2</sub>), and in the last step titanium oxide crystallized in the shell after a mild acidic chemical treatment. Finally, the silica core was removed using a NaOH solution, yielding titania hollow spheres (@TiO<sub>2</sub>). The modification @TiO<sub>2</sub> with tungstophosphoric acid (H<sub>3</sub>PW<sub>12</sub>O<sub>40</sub>) was realized by wet impregnation. The amount of TPA in the solution was fixed in order to obtain a TPA concentration of 10, 20 and 30% by weight in the final material. The system was kept at room temperature till dryness. The solids were thermally treated at 100, and 500 °C for 2 h, and will be named @TiO<sub>2</sub>TPAXX<sub>T100</sub> and @TiO<sub>2</sub>TPAXX<sub>T500</sub>, respectively, where XX is TPA concentration. The TPA content in the @TiO<sub>2</sub>TPAXX samples was estimated as the difference between the W amount contained in the tungstophosphoric acid water solution originally used for the impregnation and the amount of W that remained in the beaker after removing the dried samples. Finally, in order to remove the TPA weakly bound to the titania surface, the materials were contacted with water (typically 1 g in 1l) for 24 h, filtered, and dried at 100 °C. The amount of W in the water solutions obtained after the ground solids were extracted was determined by atomic absorption spectrometry using a Varian AA Model 240 spectrophotometer. The calibration curve method was used with standards prepared in the laboratory. The analyses were carried out at a wavelength of 254.9 nm, bandwidth 0.3 nm, lamp current 15 mA, phototube amplification 800 V, burner height 4 mm, and acetylene-nitrous oxide flame (11:14).

### 2.2. Catalyst characterization

The specific surface area of the solids was determined from N<sub>2</sub> adsorption-desorption isotherms at liquid-nitrogen temperature. They were obtained using Micromeritics ASAP 2020 equipment. The samples were previously degassed at 100 °C for 2h. Powder XRD patterns were obtained on Philips PW-1732 with built-in recorder, using Cu K $\alpha$  radiation, nickel filter, 20 mA and 40 kV in the high voltage source, and scanning angle between 5 and 60° of 2 $\theta$  at a scanning rate of 1° per minute. FT-IR spectra of the supports and catalysts were obtained in the 400-4000 cm<sup>-1</sup> wavenumber range using Bruker IFS 66 FT-IR spectrometer and pellets in KBr. Fourier transform Raman spectra were recorded on a Raman Horiba Jobin-Yvon T 64000 instrument with an Ar<sup>+</sup> laser source of 488 nm wavelength in a macroscopic configuration. The <sup>31</sup>P MAS-NMR spectra were recorded using the CP/MAS <sup>1</sup>H-<sup>31</sup>P technique with Bruker Avance II equipment. A sample holder of 4 mm diameter and 10 mm in height was employed, using 5  $\mu$ s pulses, a repetition time of 4 s and working at a frequency of 121.496 MHz for <sup>31</sup>P at room temperature. The spin rate was 8 kHz and several hundred pulse

responses were collected. Phosphoric acid 85% was employed as external reference. DRS spectra of samples were recorded using a UV-visible Lambda 35, Perkin Elmer spectrophotometer, to which a diffuse reflectance chamber with an integrating sphere of 50 mm diameter and internal Spectralon coating is attached. The range covered was 200-800 nm. The secondary electron micrographs (SEM) and the energy dispersive X-ray analysis (EDX) of the samples were obtained using a Phillips 505 Model scanning electron microscopy equipment and EDAX 9100 analyser at a working potential of 15 kV and graphite-supported samples metallized with gold.

Transmission electron microscopy (TEM) was performed in a JEOL 100 CXII microscope, working at 100 kV and at a magnification of 80000x. The samples were crushed in an agata mortar, ultrasonically dispersed in isobutanol, and deposited on a carbon-coated copper grid.

### 2.3. Catalytic test

The catalytic activity of the materials was evaluated in the photodegradation of 4-chlorophenol (4-CP) in water, at 25 °C. The tests were carried out employing 5 UV black light lamps Philips TLD 18W (emission spectra: 330–400 nm and UV intensity between 300 and 400 nm: 38 W m<sup>-2</sup>) or 5 blue fluorescent lamps Philips TLD-18W (emission spectra: 400–500 nm with UV intensity: 0.1 W m<sup>-2</sup> and global intensity between 290 and 1100 nm: 60 W m<sup>-2</sup>). UV and global intensity were monitored with a Kipp & Zonen (CM3) power meter (Omni instruments Ltd, Dundee, UK). The catalyst was maintained in suspension by stirring, and air was continuously bubbled. Previously, the 4-CP solution (100 ml, 1.5 10<sup>-4</sup> mol/l) containing 50 mg of catalyst was magnetically stirred in the absence of light for 60 min to ensure that the adsorption-desorption equilibrium of 4-CP on the surface of the materials is attained. The pH of the experiments was 6.9. During the course of them, samples were periodically withdrawn, filtered using a Millipore syringe adapter (porosity, 0.45  $\mu$ m) and then analyzed. The variation of the 4-CP concentration as a function of the reaction time was determined by a UV-visible LAMBDA 35 Perkin Elmer double-beam spectrophotometer, measuring the absorbance at 225 nm. The concentration of released chloride ions was measured by a selective Cl<sup>-</sup> electrode (pHoenix CLO1508) with an ion meter (Consort P903). The percentage of 4-CP mineralized was determined using the Total Organic Carbon, Method 10129 DR/4000 (HACH).

## 3. Results and discussion

According to the SEM micrograph (Figure. 1a), the silica cores (mean diameter in the range 650–750 nm) present a smooth surface and are well dispersed, without formation of silica aggregates. On the other hand, the SiO<sub>2</sub>@TiO<sub>2</sub> sample (Figure 1b) displays a rough surface and diameters in the range 800–900 nm.

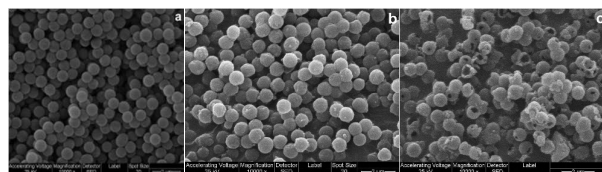


**Figure 1.** SEM micrographs SiO<sub>2</sub> (a), SiO<sub>2</sub>@TiO<sub>2</sub> (b) and @TiO<sub>2</sub> (c).

For the @TiO<sub>2</sub> material (Figure 1c), the thickness of the titania layer estimated by TEM is around 70 nm. No significant changes in the morphology of the samples after the impregnation with TPA and the thermal treatment were detected by SEM and TEM. Analyses performed by EDX show that the silica core was successfully removed using a NaOH solution. The EDX measurements (see supplementary information) revealed the presence of the Si K $\alpha$  (at 1.74 KeV) and Ti K $\alpha$  (4.51 KeV) signal in SiO<sub>2</sub>@TiO<sub>2</sub> and @TiO<sub>2</sub> samples. For SiO<sub>2</sub>@TiO<sub>2</sub> material, the ratio between the Si K $\alpha$  and Ti K $\alpha$  signal area ( $A_{SiK}/A_{TiK}$ ) was 1.43. This value was significantly lower for the @TiO<sub>2</sub> sample ( $A_{SiK}/A_{TiK}$  = 0.22), due to the almost complete silica core elimination.

The N<sub>2</sub> adsorption-desorption isotherms of @TiO<sub>2</sub>TPAXX<sub>T100</sub> and @TiO<sub>2</sub>TPAXX<sub>T500</sub> samples can be classified as type IV, characteristic of mesoporous materials. For all the materials the hysteresis loop (H2 type) was very small.

The specific surface area ( $S_{BET}$ ) of the @TiO<sub>2</sub>TPAXX<sub>T100</sub> and @TiO<sub>2</sub>TPAXX<sub>T500</sub> samples determined from N<sub>2</sub> adsorption-desorption isotherms using Brunauer-Emmett-Teller (BET) method, together with the average pore diameter ( $D_p$ ), are shown in Table 1. The specific surface area of micropores ( $S_{micro}$ ) was estimated by the t-plot method. As can be observed, all the samples are mesoporous materials with a  $D_p$  higher than 9.0 nm. The  $S_{BET}$  decreased and the mean pore radius increased when both the TPA content and the temperature of the thermal treatment were raised.

**Table 1.** Textural properties of @TiO<sub>2</sub>TPAXX materials.

Samples	$S_{BET}$ (m <sup>2</sup> /g)		$D_{pBH}$ (nm)	
	T100	T500	T100	T500
@TiO <sub>2</sub>	77	46	9.9	15.2
@TiO <sub>2</sub> TPA10	65	26	10.1	18.9
@TiO <sub>2</sub> TPA20	34	23	13.8	19.0
@TiO <sub>2</sub> TPA30	16	13	19.1	21.3

Taking into account the values of  $S_{micro}$  less than 10% of the total surface area came from a microporous structure. The XRD pattern of @TiO<sub>2</sub> calcined at 100 °C exhibited only a wide peak at  $2\theta = 25.2^\circ$  (101) assigned to the anatase phase. The XRD pattern of @TiO<sub>2</sub> treated at 500 °C also presents three new wide peaks at  $37.9^\circ$  (004),  $47.8^\circ$  (200) and  $54.3^\circ$   $2\theta$ , due to the increment of the crystallinity (see supplementary information).

On the other hand, for the @TiO<sub>2</sub>TPA10<sub>T100</sub> sample, no diffraction lines attributed to crystalline TPA or its decomposition products were present in the XRD pattern. However, a new set of peak

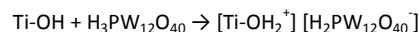
ascribed to the H<sub>3</sub>PW<sub>12</sub>O<sub>40</sub>·6H<sub>2</sub>O, (one of the more common tungstophosphoric acid hydrates) is present in XRD pattern of @TiO<sub>2</sub>TPA20<sub>T100</sub> and @TiO<sub>2</sub>TPA30<sub>T100</sub> samples.<sup>14</sup>

The patterns of the @TiO<sub>2</sub>TPA10<sub>T500</sub>, @TiO<sub>2</sub>TPA20<sub>T500</sub> and @TiO<sub>2</sub>TPA30<sub>T500</sub> samples only showed the characteristic peaks of the anatase phase; no diffraction lines corresponding to TPA were observed indicating that the species present are highly dispersed as a noncrystalline form or as crystallites low enough to be detected by this technique.

The leaching experiments revealed that TPA is firmly attached to the titania surface (less than 3% of the TPA content was eliminated). In the case of @TiO<sub>2</sub>TPA10<sub>T100</sub>, @TiO<sub>2</sub>TPA10<sub>T500</sub>, and @TiO<sub>2</sub>TPA20<sub>T500</sub> sample, the loss of TPA was practically negligible (0.90%, 0.50%, and 0.65% respectively). For all the TPA contents, the loss was lower when the samples were treated at 500 °C (for example, 2.90% and 1.75% for @TiO<sub>2</sub>TPA30<sub>T100</sub> and @TiO<sub>2</sub>TPA30<sub>500</sub>, respectively).

It is worthy to mention that the peaks in the XRD patterns of the @TiO<sub>2</sub>TPA20<sub>T100</sub> and @TiO<sub>2</sub>TPA30<sub>T100</sub> samples assigned to the H<sub>3</sub>PW<sub>12</sub>O<sub>40</sub>·6H<sub>2</sub>O, disappear as result of the leaching. We can suggest that the loosely bounded TPA eliminated during the leaching experiments was mainly the H<sub>3</sub>PW<sub>12</sub>O<sub>40</sub>·6H<sub>2</sub>O hexahydrate. In this case, hydrogen bond type interaction between oxygen atoms [W=O and W-O-W] of TPA species and hydroxyl groups [Ti-OH] of the titania matrix could take place.

However, when TPA is firmly attached to the titania surface the interaction can be of the electrostatic type due to transfer of protons to Ti-OH according to:<sup>15</sup>



Taking into account Lefebvre's report,<sup>16</sup> we can assume that the elimination of water from [Ti-OH<sub>2</sub><sup>+</sup>] during the thermal treatment should involve a direct bonding of the polyanion to titania [Ti-O-W]. Li et al. have suggested that TPA could interact with titania surfaces through Ti-O-W covalent bonds formed by the interaction of W=O or W-O-W bonds with Ti-OH species.<sup>17,18</sup>

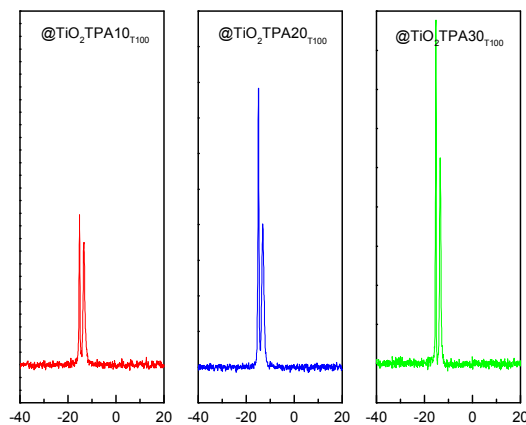


**Figure 2.** <sup>31</sup>P MAS-NMR spectra of @TiO<sub>2</sub>TPAXX<sub>T100</sub> samples.

<sup>31</sup>P MAS-NMR spectra corresponding to the @TiO<sub>2</sub>TPAXX<sub>T100</sub> (Figure 2) and @TiO<sub>2</sub>TPAXX<sub>T500</sub> materials show two signals the more intense at -14.2 ppm attributed to the [PW<sub>12</sub>O<sub>40</sub>]<sup>3-</sup> anion and the other at -12.4 ppm, to the dimer [P<sub>2</sub>W<sub>21</sub>O<sub>71</sub>]<sup>6-</sup>.<sup>19</sup> The transformation of [PW<sub>12</sub>O<sub>40</sub>]<sup>3-</sup> anion into the dimer is due to the limited stability

## ARTICLE

## Journal Name

range of the Keggin anion in solution. At pH 1.5-2, it is reversibly and quickly transformed according to the scheme:  $[PW_{12}O_{40}]^{3-} \leftrightarrow [P_2W_{21}O_{71}]^{6-} \leftrightarrow [PW_{11}O_{39}]^{7-}$  when the hydroxyl concentration is increased.<sup>20</sup>

The downfield shift and slight increase of the line width observed, compared to the bulk compound (-15.3 ppm), can be attributed to the interaction between the anion and the titania matrix<sup>21</sup> such as  $[=Ti-OH_2^+][H_{3-x}PW_{12}O_{40}]^x$ .

The <sup>31</sup>P MAS-NMR spectra of @TiO<sub>2</sub>TPAXX<sub>T500</sub> samples show that the ratio between the intensity of the signal attributed to the  $[PW_{12}O_{40}]^{3-}$  Keggin anion and the one assigned to the dimer  $[P_2W_{21}O_{71}]^{6-}$  increases with the increment of calcination temperature. We have reported<sup>3</sup> that a noticeable transformation of  $[PW_{12}O_{40}]^{3-}$  anion into the dimeric one takes place when the thermal treatment is performed at temperatures higher than 400 °C. Nevertheless, the line assigned to the  $[PW_{12}O_{40}]^{3-}$  anion is the most intense in all the samples. Additionally, the calcination at 500 °C produces a slight increment of the line with at -14.2 ppm, that could be related with the direct bonding of the polyanion to titania [Ti-O-W].

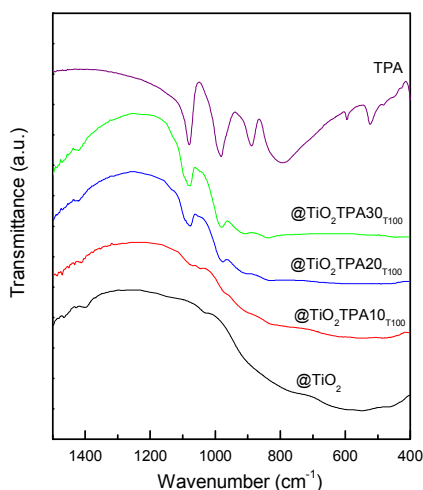


**Figure 3.** FT-IR spectra of @TiO<sub>2</sub>, TPA, and @TiO<sub>2</sub>TPAXX<sub>T100</sub> samples.

The FT-IR spectrum of TPA (Figure 3) shows bands at 1081, 982, 888, 793, 595, and 524 cm<sup>-1</sup>, in agreement with those reported in the literature for the H<sub>3</sub>PW<sub>12</sub>O<sub>40</sub> acid.<sup>22</sup> They are assigned to the stretching vibrations P-O<sub>a</sub>, W-O<sub>d</sub>, W-O<sub>b</sub>-W, W-O<sub>c</sub>-W, and to the bending vibration O<sub>a</sub>-P-O<sub>a</sub>, respectively. In the FT-IR spectra of @TiO<sub>2</sub>TPAXX<sub>T100</sub> samples, the P-O<sub>a</sub>, W-O<sub>d</sub>, and W-O<sub>b</sub>-W stretching vibrations of  $[PW_{12}O_{40}]^{3-}$  anion are overlapped to the TiO<sub>2</sub> wide band. The main FT-IR bands assigned to the stretching vibrations P-O<sub>a</sub> (1095 and 1085 cm<sup>-1</sup>), W-O<sub>d</sub> (972 cm<sup>-1</sup>), and W-O-W (890 and 790 cm<sup>-1</sup>) of the dimer  $[P_2W_{21}O_{71}]^{6-}$ , appear at wavenumber values similar to those of the  $[PW_{12}O_{40}]^{3-}$  Keggin anion.<sup>23</sup> For the @TiO<sub>2</sub>TPA20<sub>T100</sub> and @TiO<sub>2</sub>TPA30<sub>T100</sub> samples the band at 1080 cm<sup>-1</sup>, displays a shoulder (at 1094 cm<sup>-1</sup>) assignable to the presence of the  $[P_2W_{21}O_{71}]^{6-}$  anion.

From FT-IR and <sup>31</sup>P MAS-NMR results, we can state that main species present in the samples is the  $[PW_{12}O_{40}]^{3-}$  Keggin anion. However, it was partially transformed into  $[P_2W_{21}O_{71}]^{6-}$  dimer during the synthesis and drying steps.

The main Raman vibration bands of bulk TPA appear at 1010, 990 and 930 cm<sup>-1</sup>.<sup>24</sup> They present an important broadening when TPA is

supported on @TiO<sub>2</sub>. Additionally, in the spectra of @TiO<sub>2</sub>TPAXX<sub>T500</sub> samples, the main Raman scattering peak of TiO<sub>2</sub> at 141 cm<sup>-1</sup> exhibits a strong blue shift and broadening. In agreement with Li et al.<sup>25</sup> we consider that the shift and broadening of the Raman vibration modes of TPA and TiO<sub>2</sub> could be associated with a strong interaction between the TiO<sub>2</sub> network and TPA.

The UV-vis-DRS spectrum of bulk TPA presented two absorption bands in the range 200–450 nm, assigned to the charge transfer from bridging or terminal O 2p to W 5d (W-O-W and W-Od, respectively).<sup>3</sup> On the other hand, @TiO<sub>2</sub> sample displayed intense absorption in the range 200–390 nm, corresponding to charge transfer from the valence band (O 2p) to the conduction band (Ti 3d).<sup>26</sup>

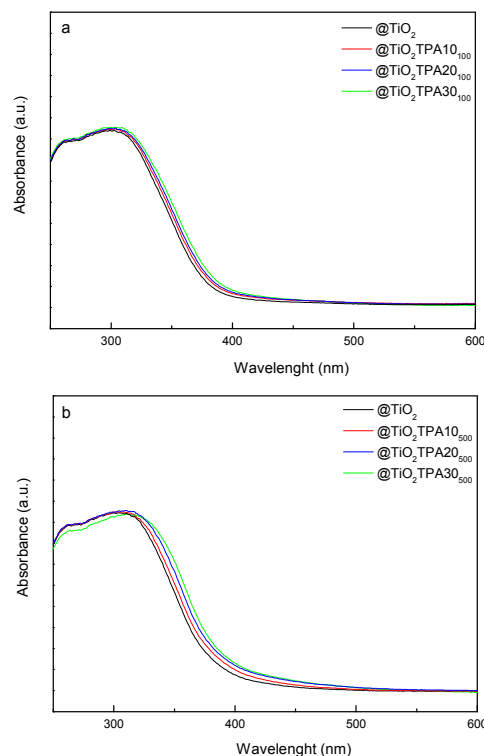


**Figure 4.** DRS spectra of @TiO<sub>2</sub>, and @TiO<sub>2</sub>TPAXX samples calcined at 100 (a) and 500 °C (b).

The UV-vis-DRS spectra of @TiO<sub>2</sub>TPAXX<sub>T100</sub> and @TiO<sub>2</sub>TPAXX<sub>T500</sub> samples (Figure 4a y 4b respectively) show an absorption threshold onset that continuously shifts to the visible region with the increment of TPA content. DRS results also reveal that the visible light absorption increases when the calcination temperature was raised up to 500 °C. So, the TPA-TiO<sub>2</sub> surface complex could be responsible for the visible light absorption and spectroscopic changes observed.

We evaluated the activity of synthesized materials in the photocatalytic degradation of 4-chlorophenol at the pH of the suspension obtained by the addition of catalyst to 4-CP water solution. The initial and the final pH of the solutions were in the range 6.9-5.7.



The point of zero charge ( $\text{pH}_{\text{PZC}}$ ) of the @TiO<sub>2</sub>TPAXX<sub>T100</sub> samples (estimated using the mass titration method proposed by Noh and Schwarz<sup>27</sup>) decreases in the following order: @TiO<sub>2</sub>TPA10<sub>T100</sub> (5.4) > @TiO<sub>2</sub>TPA20<sub>T100</sub> (4.9) > @TiO<sub>2</sub>TPA30<sub>T100</sub> (4.3) due to the incorporation of TPA. In the case of the samples treated at 500 °C, the behaviour is the same: @TiO<sub>2</sub>TPA10<sub>T500</sub> (5.2) > @TiO<sub>2</sub>TPA20<sub>T500</sub> (4.1) > @TiO<sub>2</sub>TPA30<sub>T500</sub> (2.7). However, the values are slightly lower than those of the @TiO<sub>2</sub>TPAXX<sub>T100</sub> samples, due to the elimination of water from [Ti-OH<sub>2</sub><sup>+</sup>] during the thermal treatment. So, under our experimental conditions, the surface of the @TiO<sub>2</sub>TPAXX samples was mostly negatively charged. As a result, 4-CP is not significantly adsorbed on the catalyst surface.

Experiments made without catalyst (under UV-A and visible irradiation), showed negligible 4-CP degradation after 240 min of irradiation.

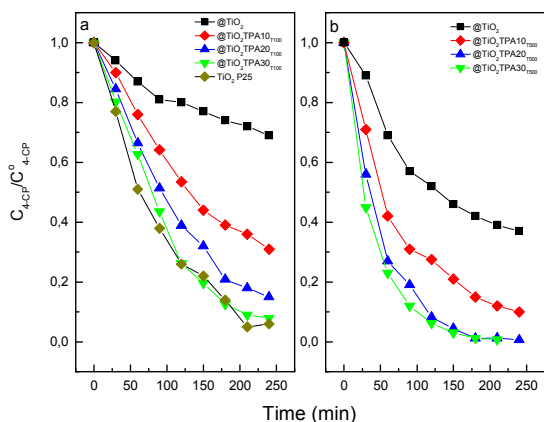


**Figure 5.** Photocatalytic degradation of 4-CP as a function of the time (under UV-A irradiation) for @TiO<sub>2</sub>, @TiO<sub>2</sub>TPAXX samples treated at 100°C (a), 500°C (b), and TiO<sub>2</sub> Evonik P25.

The variation of 4-CP concentration as a function of time using the @TiO<sub>2</sub>TPAXX<sub>T100</sub> and @TiO<sub>2</sub>TPAXX<sub>T500</sub> catalysts is shown in Figure 5. The reduction in the 4-CP concentration was rather low (31%) for the titania hollow spheres treated at 100 °C after 240 min of irradiation. However, 4-CP degradation significantly increases in parallel with the increment of tungstophosphoric acid: @TiO<sub>2</sub>TPA10<sub>T100</sub> (69%) < @TiO<sub>2</sub>TPA20<sub>T100</sub> (85%) < @TiO<sub>2</sub>TPA30<sub>T100</sub> (92%). This behavior is due to the fact that TPA on the TiO<sub>2</sub> surface acts as an effective trap of photoinduced electrons. Electrons can be easily transferred from the TiO<sub>2</sub> conduction band to TPA Keggin anions on the surface, decreasing the fast e<sup>-</sup>/h<sup>+</sup> recombination,<sup>28</sup> and leaving more valence band holes (h<sup>+</sup>VB) available to react with water molecules to yield <sup>•</sup>OH radicals.

Additionally, the increment of the catalytic activity could be due to the direct participation of TPA in the degradation of the organic substrate.<sup>3</sup> TPA absorb strongly in the UV region of the light spectrum ( $\lambda < 400$  nm). This absorption corresponds to the ligand-to-metal charge-transfer band and it can generate strongly oxidizing excited state TPA\*. They can perform the oxidation of organic substrates directly via charge transfer or indirectly through the production of <sup>•</sup>OH reactive species that participates in the degradation of the organic substrate.<sup>29,30</sup> After that, the corresponding reduced TPA<sup>-</sup> are usually reoxidized to their original oxidation state by an electron acceptor such as dioxygen.

The degradation profile of 4-CP using TiO<sub>2</sub> Evonik P25 (commonly used as reference) was very similar to that of the @TiO<sub>2</sub>TPA30<sub>T100</sub> sample.

Figure 5b shows that the 4-CP amount degraded after 240 min of UV irradiation, increased when the calcination temperature was raised up to 500 °C. For any TPA content considered, we observed that the 4-CP degraded amount of increases with the increment of calcination temperature (i.e., @TiO<sub>2</sub>TPA10<sub>T500</sub> (90%) > @TiO<sub>2</sub>TPA10<sub>T100</sub> (69%)). This can be due to an increase in the crystallinity of the @TiO<sub>2</sub>, resulting in a decrease in the number of defects that act as recombination centers for photogenerated electrons and holes.

For @TiO<sub>2</sub>TPAXX<sub>T100</sub> and @TiO<sub>2</sub>TPAXX<sub>T500</sub> samples, we observed that the ratio between the amount of degraded 4-CP and the amount of released chloride ions as a function of the irradiation time remains practically equal to 1 during the course of the degradation. These results are in concordance with literature reports that evidence that the first step during the photocatalytic degradation of 4-CP, is the cleavage Cl-aryl bond.

On the other hand, we found that the 4-CP amount degraded under blue-light irradiation (at 240 min), using titania hollow spheres modified with TPA as catalyst, varies in the following way: @TiO<sub>2</sub>TPA10<sub>T500</sub> (20%) < @TiO<sub>2</sub>TPA20<sub>T500</sub> (27%)  $\cong$  @TiO<sub>2</sub>TPA30<sub>T500</sub> (29 %). On the contrary, the catalytic activities of Evonik P25 and @TiO<sub>2</sub> were negligible. These results show the beneficial effect of TPA on the photocatalytic activity also under visible light radiations.

Under visible light irradiation the TPA anchored to the titania surfaces through Ti-O-W covalent bonds (responsible for the visible light absorption) would be excited yielding TPA\*-TiO<sub>2</sub> complex. The TPA\*-TiO<sub>2</sub> complex can inject a photoexcited electron to the TiO<sub>2</sub> CB.<sup>31-33</sup> Electron injection from TPA in the excited state (TPA\*) to the CB of TiO<sub>2</sub> was clearly observed using the two-color two-laser flash-photolysis technique.<sup>33</sup>

The electron injected to TiO<sub>2</sub> CB can react with molecular oxygen yielding a <sup>•</sup>O<sub>2</sub><sup>-</sup> radical. It is well known that in aqueous media this radical can undergo disproportion reactions producing mainly hydrogen peroxide.<sup>34</sup> H<sub>2</sub>O<sub>2</sub> can be also reduced by CB electrons producing <sup>•</sup>OH radicals that are also able to oxidize organic pollutants.

Nevertheless, the generation of hydrogen peroxide by means of disproportion of <sup>•</sup>O<sub>2</sub><sup>-</sup> radicals is very low in irradiated TiO<sub>2</sub> surfaces,<sup>35,36</sup> which should account for the low degradation of 4-CP.

It is worthy to mention that the @TiO<sub>2</sub>TPA samples can be easily separated from the resulting suspension by decantation. On the contrary, Evonik P25 can be recovered only by filtration using Millipore filters. Taking into account the obtained results, @TiO<sub>2</sub>TPA30<sub>T500</sub> was chosen to test its reusability. To this end, after each photocatalytic experiment, the catalyst was easily separated from the resulting suspension by decantation, washed with distilled water, dried at 70 °C and reused four times (under UV-A irradiation).

The percentage of 4-CP degraded decrease slightly during the first and the second reuse (95% and 91% respectively), and then keep constant. The decrease could be assigned to the TPA solubilization (less than 1% of the TPA content), as was established by atomic absorption spectrometry. On the other hand, the mineralization

## ARTICLE

## Journal Name

degree was slightly lower than the amount of degraded 4-CP (78 % and 70% for the first and the second reuse respectively) as a result of the formation of organic intermediates such as benzoquinone and hydroquinone.<sup>37</sup>

The activity of @TiO<sub>2</sub>TPA solids in the degradation of 4-chlorophenol aqueous solutions under UV and visible light irradiation increases with the TPA content and the thermal treatment temperature. The sample containing 30% TPA and annealed at 500 °C showed the highest photocatalytic activity. Furthermore, the reused catalysts showed only a slight decrease in the degradation and mineralization degree, thus being promissory materials to aid in the photocatalytic treatment of wastewater containing chlorinated phenols.

## Conclusions

Titania hollow spheres were synthesized by the sol-gel method using silica nanospheres as template. The direct modification of @TiO<sub>2</sub> with tungstophosphoric acid enables obtaining visible-light-absorbing materials. This fact could be due to the generation of surface complexes between TPA anions and TiO<sub>2</sub> through the formation of Ti-O-W bonds. Due to the formation of these bonds the main Raman scattering of TPA and TiO<sub>2</sub> displayed a strong blue shift and broadening.

FT-IR and <sup>31</sup>P MAS-NMR results indicated that the main species present in the samples is the [PW<sub>12</sub>O<sub>40</sub>]<sup>3-</sup> anion, which was partially transformed into the [P<sub>2</sub>W<sub>21</sub>O<sub>71</sub>]<sup>6-</sup> dimeric anion during the synthesis and thermal treatment steps.

@TiO<sub>2</sub>TPA materials exhibit higher photocatalytic activity than @TiO<sub>2</sub> under UV-A irradiation, since the TPA acts as a sink of conduction band photo-induced electrons decreasing the e<sup>-</sup>/h<sup>+</sup> recombination leaving available more valence band holes to either directly oxidize malachite green molecules or produce •OH radicals. Visible light photocatalytic activity of these materials in the 4-CP degradation could be explained by the fact that TPA-TiO<sub>2</sub> complex may be excited by visible light absorption and inject an electron into the TiO<sub>2</sub> conduction band, inducing the indirect formation of •OH radicals.

Finally, the direct modification of @TiO<sub>2</sub> with TPA is a good method to obtain catalysts with photocatalytic activity in the 4-chlorophenol degradation under UV-A and visible light irradiation.

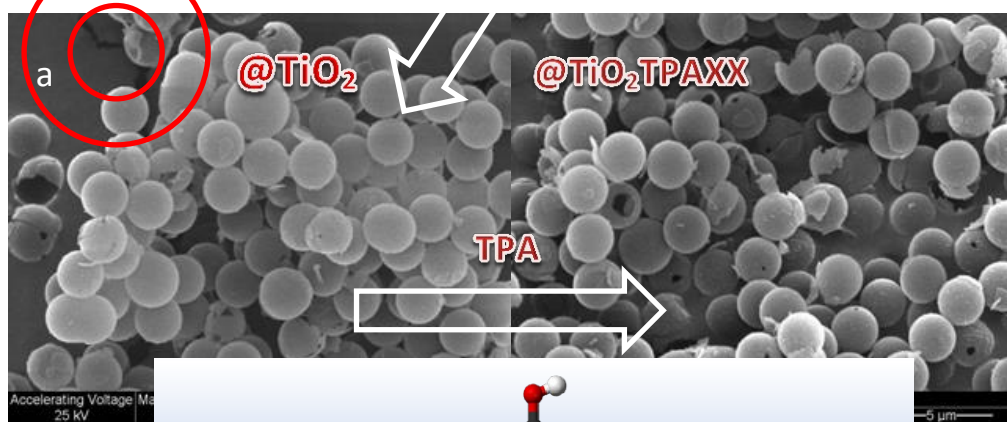
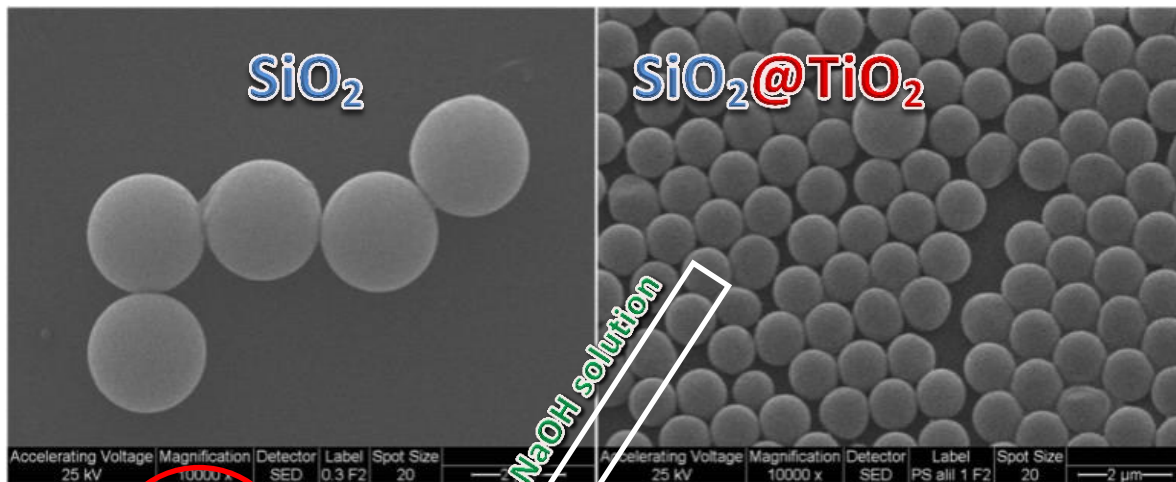
## Acknowledgements

Authors thank the financial support from CONICET (PIP 628) and Universidad Nacional de La Plata (UNLP) (Project number X638) and the technical assistance of M. Theiller (SEM/EDX analysis) and P. Fetsis (BET).

## References

- M.R. Hoffmann, S.T. Martin, W. Choi and D.W. Bahnemann, *Chem. Rev.*, 1995, **95**, 69-96.
- T. Ochiai and A. Fujishima, *J. Photoch. Photobiol. C.*, 2012, **13**, 247-262.
- M.N. Blanco and L.R. Pizzio, *Appl. Catal. A: Gen.*, 2011, **405**, 69-78.
- K.B. Kyoko, S. Kazuhiro, K. Hitoshi, O. Kiyomi and A. Hironori, *Appl. Catal. A: Gen.*, 1997, **165**, 391-409.

- J.G. Yu, W. Liu and H.G. Yu, *Cryst. Growth Des.*, 2008, **8**, 930.
- C. Jia, Y. Cao and P. Yang, *Funct. Mater. Lett.*, 2013, **6**, 1350025-6.
- C. Liu, H. Yin, L. Shi, A. Wang, Y. Feng, L. Shen, Z. Wu, G. Wu and T. Jiang, *J. Nanosci. Nanotechnol.*, 2014, **14**, 7072-7078.
- L. Yan, X. He, Y. Wang, J. Li and D. Wang, *J. Mater. Sci: Mater Electron*, 2016, **27**, 4068-4073.
- L. Li, S. Bai, W. Yin, S. Li, Y. Zhang and Z. Li, *Int. J. Hydrogen Energ.*, 2016, **41**, 1627-1634.
- A.L. Di Virgilio, I. Maisuls, F. Kleitz and P.M. Arnal, *J. Colloid Interface Sci.*, 2013, **394**, 147-156.
- C. Castañeda, F. Tzompantzi, R. Gómez and Hugo Rojas, *J. Chem. Technol. Biotechnol.*, 2016, **91**, 2170-2178.
- M. Wang, G. Fang, P. Liu, D. Zhou, C. Ma, D. Zhang, J. Zhan, *Appl. Catal. B: Environ.*, 2016, **188**, 113-122.
- Y. Yao, L. Jiao, N. Yu, J. Zhu and X. Chen, *Russ. J. Electrochem.* 2016, **52**, 348-354.
- J.B. Mioc, R.Z. Dimitrijevi, M. Davidovic, Z.P. Nedic, M.M. Mitrovic and P.H.Colomban, *J. Mater. Sci.*, 1994, **29**, 3705-3718.
- V.M. Fuchs, E.L. Soto, M.N. Blanco and L.R. Pizzio, *J. Colloid Interfaces Sci.*, 2008, **327**,403-411.
- F. Lefebvre, *J. Chem. Soc. Chem. Commun.*, 1992, **10**, 756-757.
- K. Li, Y. Guo, F. Ma, H. Li and L. Chen, *Y. Guo, Catal. Commun.*, 2010, **11**, 839-843.
- K. Li, X. Yang, Y. Guo, F. Ma, H. Li and L. Chen, *Y. Guo, Appl. Catal. B Environ.*, 2010, **99**, 364-375.
- M.T. Pope, *Heteropoly and Isopolyoxometalates*, Springer-Verlag, Heidelberg, 1983, pp. p58.
- R. Massart, R. Contant, J. Fruchart, J. Ciabrini and M. Fournier, *Inorg. Chem.*, 1977, **16**, 2916.
- V.M. Mastikhin, S.M. Kulikov, A.V. Nosov, I.V. Kozhevnikov, I.L. Mudrakovsky and M.N. Timofeeva, *J. Mol. Catal. A Chem.*, 1990, **60**, 65-70.
- C. Rocchiccioli-Deltcheff, R. Thouvenot and R. Franck, *Spectrochim. Acta*, 1976, **32A**, 587-597.
- R. Contant, *Can. J. Chem.*, 1978, **65**, 568-573.
- I. Holclajtner-Antunovic, D. Bajuk-Bogdanovic, A. Popa and S. Uskokovic-Markovic, *Inorg. Chim. Acta*, 2012, **383**, 26-32.
- J. Li, W. Kang, X. Yang, X. Yu, L. Xu, Y. Guo, H. Fang and S. Zhang, *Desalination.*, 2010, **255**, 107-116.
- J.T. Yates, *Surf. Sci.*, 2009, **603**, 1605-1612.
- J.S. Noh and J.A. Schwarz, *J. Colloid Interface Sci.*, 1988, **130**, 157-164.
- H. Park and W. Choi, *J. Phys. Chem.B*, 2003, **107**, 3885.
- R.R. Ozer and J.L. Ferry, *J. Phys. Chem. B*, 2000, **104**, 9444.
- S. Antonaraki, T.M. Triantis, E. Papaconstantinou and A. Hiskia, *Catal. Today*, 2010, **151**, 119-124.
- R. Sivakumar, J. Thomas and M. Yoon, *J. Photochem. Photobiol. C: Rev.*, 2012, **13**, 277-298.
- J.A. Rengifo-Herrera, M.N. Blanco and L.R. Pizzio, *Mater. Res. Bull.*, 2014, **49**, 618-624.
- T. Tachikawa, S. Tojo, M. Fujitsutka and T. Majima, *Chem. Eur. J.*, 2006, **12**, 3124-3131.
- D.T. Sawyer and J.S. Valentine, *Chem. Res.*, 1981, **14**, 393-400.
- Y. Nosaka, Y. Yamashita and H. Fukuyama, *J. Phys. Chem. B*, 1997, **101**, 5822-5827.
- H. Sakai, R. Baba, K. Hashimoto, A. Fujishima, A. Heller, *J. Phys. Chem. B*, 1995, **99**, 11896-11900.
- A. Mylonas and E. Papaconstantinou, *J. Photochem. Photobiol. A.*, 1996, **94**, 77-82.



A diagram illustrating the process of 4-chlorophenol photodegradation. It features a colorful lightning bolt icon on the left, a ball-and-stick molecular model of 4-chlorophenol in the center, and a blue box on the right containing the text "4-chlorophenol photodegradation". Below these elements, a blue box contains the text "visible-light-absorbing materials".